Arsenic speciation in multiple metal environments: I. Bulk-XAFS spectroscopy of model and mixed compounds

Markus Gräfe [a,*,1], Ryan V. Tappero [a], Matthew A. Marcus [b], Donald L. Sparks [a]

[a] *Environmental Soil Chemistry Group, Department of Plant & Soil Sciences, 152 Townsend Hall, University of Delaware, Newark, DE 19716, USA*
[b] *Advanced Light Source, Beamline 10.3.2, Lawrence Berkeley National Laboratories, Berkeley, CA 94720, USA*

Received 6 September 2007; accepted 18 January 2008

Available online 25 January 2008

Abstract

X-ray absorption fine structure (XAFS) spectroscopy was employed to determine the bonding environment of As(V) in the presence of Cu(II) and Zn(II) on goethite and gibbsite. In addition, several mineral species and precipitates derived from homogeneous and heterogeneous (presence of α-Cr_2O_3) super-saturations were studied. Structural parameters were determined after resolving the broad second shells in r-space by differential k-weighting (1, 2 or 3) and k-ranging (2.5- vs 3.5–12.75 Å) of the raw EXAFS functions. In precipitates, AsO_4 was incorporated in the metal-hydroxides forming clinoclase-like and koettigite-like structures in the presence of Cu(II) and Zn(II), respectively. In the presence of both Cu(II) and Zn(II), the clinoclase structure formed preferentially over the koettigite structure under homogeneous oversaturated solution conditions and in the presence of eskolaite (α-Cr_2O_3). Silica promoted the formation of koettigite-like zinc-arsenate precipitates from initial As(V) and Zn(II) solution concentrations of 500 μM. On goethite and gibbsite, 750 μM As(V) formed mainly bidentate binuclear surface species in accordance with many previous findings even in the presence of equimolar Cu(II) and or Zn(II) concentrations. Copper was readily identified in the second shell environment of As(V) sorbed on gibbsite, but not on goethite. We hypothesize that this complex formed on the basis of Cu(II)'s ability to form polymeric species in solution and at the mineral–water interface in agreement with previous studies. The effects of Zn(II) on the coordination environment of As(V) on gibbsite and goethite could not be ascertained with As K-edge EXAFS spectroscopy. In addition to bidentate binuclear surface complexes, As(V) formed edge-sharing complexes with Fe, Al, and Cu atoms, which we could differentiate on the basis of the inter-atomic distances, phase shifts between wavefunctions of Fourier-filtered peaks, and differences in amplitude of the absorption envelopes. The analyses showed that of all data reduction steps, data presented in r-space and as wavefunctions of Fourier-filtered shells offer the greatest possibility for fingerprinting and inferring the influence of co-sorbing metal cations on the As(V) sorption complex. With regards to interpretations of micro-EXAFS data by abstract factor analyses and linear least-square combination fitting, analyses of As K-edge data should not be performed on the raw $\chi(k)$ data, but rather on consistently isolated second and higher-order shell features.
© 2008 Elsevier Inc. All rights reserved.

Keywords: Copper; Zinc; Goethite; Gibbsite; EXAFS spectroscopy; Phase shifts; Edge-sharing complexes

1. Introduction

Arsenic is a toxic metalloid whose chemical speciation and toxicity are dependent on the redox potential and pH. In oxidized environments, arsenate [$H_{3-n}AsO_4^{0-n}$ = As(V)], the less toxic species, is prevalent, whereas in suboxic environments, arsenite [$H_{3-n}AsO_3^{0-n}$ = As(III)], the more toxic species, is dominant [1–3]. The fate of arsenic in contaminated environments is directly related to this basic differentiation of chemical species, because their symmetry ($As(V)_{tetrahedral}$ vs $As(III)_{bipyramidal}$), acid/base behavior, charge and affinity to other elements such as Al, Fe, Cu, Zn, S, and C are fundamentally different [1,4]. To date, the solid phase formation of As(V) and As(III) species has been studied extensively for single ion-surface systems and specifically for the variable charged surfaces of the Fe- and Al-oxides (e.g., goethite, ferrihydrite, gibbsite, boehmite) [5–10]. Arsenate is coordinated at these

* Corresponding author. Fax: +61 2 9351 5108.
E-mail address: m.grafe@usyd.edu.au (M. Gräfe).
[1] Current address: Faculty of Agriculture, Food & Natural Resources, Ross Street Building (A03), Room 322, The University of Sydney, NSW 2006, Australia.

surfaces by two hydroxyl (OH) functional groups extending from metal polyhedra (e.g., $Fe(OH)_3 \cdot 3H_2O$). This surface complex is known as the bidentate binuclear or double-corner sharing complex ($^2C_{As–Fe/Al}$) and forms as a result of a ligand exchange reaction [5,11]. On goethite (α-FeOOH), the bidentate binuclear sorption complex is identified by a characteristic As–Fe distance ($R_{As–Fe}$) between 3.26 and 3.32 Å and a coordination number (N) magnitude between one and two. On gibbsite ($Al(OH)_3$), the bidentate binuclear complex is identified by $R_{As–Al} \sim 3.15$ Å with a similar magnitude for N as on goethite [12]. This surface complex has been corroborated by other spectroscopic evidence (Fourier transform infrared, FTIR spectroscopy) for ions with tetrahedral symmetry (e.g., PO_4), and by modeling the sorption reaction using the constant capacitance model [13–15]. A second surface complex on goethite was suggested by Fendorf et al. and Manceau in which As(V) is coordinated by two O atoms that are part of the same metal octahedron [5,16]. This surface complex, referred to as the bidentate mononuclear or edge-sharing surface complex ($^1E_{As–M,\,M=metal}$) was recently analyzed by Sherman and Randall [17] who argued on the basis of density functional theory (DFT) calculations on a small $Fe_2(OH)_2 \cdot 8H_2O$ cluster that the $^1E_{As–Fe}$ complex was energetically unfavorable. Modeling extended X-ray absorption fine structure (EXAFS) data of As(V) sorbed on goethite, the authors suggested that contributions to the EXAFS spectra expressed at $R + \Delta R \sim 2.85$ Å stemmed solely from non-collinear multiple scattering (MS) in the As(V) tetrahedron in addition to the bidentate binuclear configuration of As(V) on the goethite surface. Ladeira et al. also dismissed the formation of $^1E_{As–Al}$ complexes based on their DFT calculations on a small $Al_2(OH)_2 \cdot 8H_2O$ cluster [12]. Observations of multiple scattering (MS) for ions in tetrahedral coordination have been made by Pandya [18] for chromate [Cr(VI)] and by Foster et al. and Gräfe and Spaks for As(V) [19–21]. In our own research, the MS feature for aqueous (outer-sphere), sorbed, precipitated and mineralized species ranged between 3.10 and 3.23 Å with an average coordination number (CN) of 18.9 [20]. In relation to the two proposed surface complexes (^1E and ^2C), $R_{As–Fe/Al,\,1E} < R_{MS} < R_{As–Fe/Al,\,2C}$ suggesting that the broad second shell feature in Fourier transforms (FTs) of As(V) sorbed on Fe and Al oxides is possibly a composite of the ^1E complex, MS and the ^2C complex. As foreign metal cations are introduced to the surface, the ^2C and ^1E complexes may form on mixed edge-sharing octahedra (e.g., Fe–Cu or Fe–Zn). Indeed, the edge-sharing complex of metal cations on Fe and Al oxides is the dominant surface complex at and below monolayer coverage [20,22–26]. An unambiguous differentiation of the second shell metal in As(V) spectra is however quite difficult, with some indicators given only by the position of the imaginary part in the FT [26]. Recently, we showed that proton (H^+) promoted desorption of As(V) from 6-month old co-sorbed As(V) and Zn(II) fractions on goethite was greater in the presence of Zn(II, as opposed to its absence under the same ageing conditions) suggesting that some of the surface adsorbed As(V) was coordinated by Zn(II) [20]. Raw k^3-weighted $\chi(k)$ spectra and FTs however could not confirm the presence or absence of Zn(II) in the second shell.

This study analyzed EXAFS data of more than 20 As sorption samples and mineral standards and discriminated among spectral analyses steps (XANES vs raw k^3-weighted $\chi(k)$ vs FTs vs individually Fourier filtered shell contributions [$k^3 \cdot \chi(k)$]) for the greatest spectral differences upon visual inspection and upon non-linear least-square shell fitting. The analyses were performed for spectra collected on As(V) sorption complexes on goethite and gibbsite in the presence and absence of copper [Cu(II)] and or zinc [Zn(II)], on freshly precipitated Cu- and Zn-arsenate precipitates in the presence and absence of α-Cr_2O_3 (s), on several mineral species such as scorodite ($FeAsO_4$), olivenite ($Cu_2[AsO_4]OH$) and adamite ($Zn_2[AsO_4]OH$), and an aqueous Na_2HAsO_4 sample. It supports an investigation into the influence of co-sorbing metals (Cr, Cu and Zn) on the solid phase speciation of arsenic (As) in a copper-chromated-arsenate (CCA) contaminated soil using *in situ* synchrotron-based, micro-focused X-ray absorption spectroscopy (μXAS). The detailed analyses presented in this paper were warranted for several reasons: (1) As(V)'s solid phase speciation in soils and sediments is greatly influenced by the presence and variety of sorbing surfaces (e.g., goethite vs gibbsite), pH, redox potential and presence of co-sorbing metals (e.g., Cu and Zn) and other ligands (e.g., PO_4) [2,20,26]. (2) The number and type of structural elements (e.g., edge-sharing vs corner-sharing complexes) comprising As(V)'s second shell ($R + \Delta R$ 2.20 Å, uncorrected for phase shifts) and possible contributions from MS remain unclear for As(V) surface complexes on Fe and Al oxides [10,16,17,27]. (3) It is unclear whether co-sorbing metals (e.g., Cu and Zn) other than Fe and or Al can be unambiguously identified in As(V)'s second shell especially when no (surface) precipitate has formed and the ions co-exist on the same surface; and (4) detailed statistical analyses (principal component analysis (PCA), target transformation (TT) and linear least-square combination fit (LLSF) analysis) of μEXAFS spectra collected from heterogeneous soil samples require a suite of known reference compounds and should be conducted at a spectral analysis step that provides the greatest measurable differences.

2. Materials and methods

2.1. Sample preparation

Table 1 lists sorption, precipitate, mineral and aqueous samples and provides a brief tabulated description on how sorption and freshly precipitated samples were prepared. Mineral species were obtained from *Excalibur*™ (Peekskill, NY). X-ray diffraction data was collected to verify the presence and purity of the minerals. The suspension density of goethite and gibbsite were adjusted such that each suspension density in solution was equal to 70 $m^2 L^{-1}$ 0.01 M NaCl. The reaction pH was held constant at 7.0 using 0.1 or 1.0 M NaOH or HCl and a pH stat. Incremental additions of 250 μM of As(V), Cu(II) and or Zn(II) were administered at minimum 0.5 h intervals or until the change in pH was equal to zero (whichever came later). The equilibration period for all samples was equal to 24 h after the final reactant was ap-

Table 1
Sample preparation, surface loading and nomenclature

Reference	pH	Sorbent	As(V) (mM)	Cu/Zn (mM)	# incr.[a]	As/Cu/Zn Γ (μmol m^{-2})
Solutions						
Na_2HAsO_4(aq.)	7.0	0.01 M NaCl	25	0/0	1	25 mM
Sorption samples						
AsGoe_1d[b]	7.0	Goethite	0.25	0/0/0.25	1	1.08/0/0
AsGoe_1mo[b]	7.0	Goethite	0.25	0/0/0.25	1	2.20/0/0
AsCuGoe	7.0	Goethite	0.25	0/0/0.25	3	1.85/4.25/0
AsZnGoe	7.0	Goethite	0.25	0/0/0.25	3	2.68/0/3.10
AsCuZnGoe	7.0	Goethite	0.25	0/0/0.25	3	2.71/4.23/2.92
AsGib_1d	7.0	Gibbsite	0.25	0/0	1	0.98
AsGib_aged[b]	7.0	Gibbsite	0.25	0/0	1	
AsCuGib	7.0	Gibbsite	0.25	0.25/0	3	2.41/5.63/0
AsZnGib	7.0	Gibbsite	0.25	0/0.25	3	2.32/0/2.91
AsCuZnGib	7.0	Gibbsite	0.25	0.25/0.25	3	2.44/5.34/2.82
$AsZnSiO_2$[c]	7.0	SiO_2	0.50	0/0.5	2	8.2/0/8.7
Homogeneous precipitates						
CuAsPrecip.	7.00	0.01 M NaCl	10	10/0	1	
ZnAsPrecip.	7.00	0.01 M NaCl	10	0/10	1	
CuZnAsPrecip.	7.00	0.01 M NaCl	10	10/10	1	
Heterogeneous precipitates			α-Cr_2O_3			
Cr–CuAsPrecip.	7.00	0.01 M NaCl	10	10/0/10	1	
Cr–ZnAsPrecip.	7.00	0.01 M NaCl	10	0/10/10	1	
Cr–CuZnAsPrecip.	7.00	0.01 M NaCl	10	10/10/10	1	
Minerals						
Adamite	$Zn_2(AsO_4)OH$					
Chalcophyllite	$Cu_9Al(AsO_4)_2(SO_4)_{1.5}(OH)_{12}\cdot 18H_2O$					
Olivenite	$Cu_2(AsO_4)OH$					
Ojuelaite	$ZnFe_2^{3+}(AsO_4)_2(OH)_2\cdot 4H_2O$					
Scorodite	$FeAsO_4\cdot 2H_2O$					

[a] The number of increments refers to how many times a certain concentration was applied to the reaction, e.g., for AsCuGoe, 3 increments of 0.25 mM As(V) and Cu(II) were made. The equilibration period between each increment was $\geqslant$0.5 h or until the δpH/δtime = 0. The samples were then aged for an additional 24 h.

[b] AsGoe_1d and AsGib_1d were equilibrated for one day, whereas AsGoe_1mo was equilibrated for 1 month. Originally believed to be mansfieldite ($AlAsO_4$). XRD however revealed an amorphous phase.

[c] Listed with precipitates in Table 3 and discussed as a precipitate.

plied except were noted (e.g., AsGoe_1mo was equilibrated for 1 month).

2.2. EXAFS data collection

The majority of EXAFS data were collected at beamline X-11A (National Synchrotron Light Source, Brookhaven National Laboratory, Upton NY) with some data collected at beamline 10.3.2 (Advanced Light Source, Lawrence Berkeley National Laboratories, Berkeley CA). The operational details for both beamlines have been described in detail elsewhere [20,28]. All spectra were collected at the As K-edge (11.868 keV). At least three scans per sample were collected in order to improve the signal to noise ratio. EXAFS data for sorption samples were collected using a Lytle detector as well as some of the precipitated samples. Mineral and aqueous samples were collected in transmission mode. Further details of the data acquisition are described elsewhere [20,26].

2.3. EXAFS data analysis

All data reduction was performed with WinXAS 2.3 and later versions [29] using standard procedures described elsewhere [30]. Briefly, individual energy spectra were corrected for shifts in edge energy and a pre- and post-edge background was subtracted from the energy functions for normalization prior to averaging. Averaged spectra were converted from energy to photo-electron wave vector (k) units (k = is the wave vector number with units of $\sim$ Å^{-1}) by assigning the origin, E_0, to the first inflection point of the absorption edge (As(V) = 11.874 keV). The EXAFS oscillations were extracted using a cubic spline function consisting of $\leqslant$7 knots applied over an average range in k-space (As: 2.0–13.0 Å^{-1}). Fourier transformation of the raw $\chi(k)$ function was performed over two k-ranges (As: 2.50– and 3.50–12.75 Å^{-1}) at k^1-, k^2- and k^3-weighting to obtain radial structure functions (RSFs or r-space) using a Bessel window function and a smoothing parameter (β) of 4 to minimize truncation effects in r-space. This procedure

[*vide infra*] is capable of suppressing contributions from MS allowing for an improved isolation of the major second shell peak and is consistent with previous findings [18]. Peaks in the FTs were then converted back to k-space (Å^{-1}) for non-linear least-square shell fitting. Contributions to the EXAFS signal from MS and possible ^{1}E surface complexes were isolated after Fourier transforming a k^2-weighted range of 2.5 to 12.75 Å^{-1} and converting the resultant r-space ($R + \Delta R$, Å) from 2.20 to 2.70 Å back into k-space (Å^{-1}). The second shell's major peak was initially isolated after Fourier transforming a k^3-weighted k-range of 2.5 to 12.75 Å^{-1}, and Fourier back-transforming r-space between 2.5 and up to 3.9 Å (depending on the breadth of the second shell feature(s)) into k-space (Å^{-1}). Although Fourier transformation of a k-range between 3.5 and 12.75 Å^{-1} improved the resolution of the FT peaks in samples based on goethite and gibbsite, the As–Al amplitude functions of gibbsite-based samples were prone to lose amplitude if the lower end of the k-range was increased to 3.5 Å^{-1}. For the sake of consistency, all raw EXAFS data were therefore Fourier transformed between 2.5 and 12.75 Å^{-1}. In order to determine the influence of contributions from MS and possible ^{1}E complexes on the Fourier back-transformed $\chi(k)$ functions, several ranges in r-space were probed [*vide infra*]. Second shell contributions to the EXAFS were best isolated when the lower r-range was $\geqslant$2.5 Å (uncorrected for phase shifts).

The FEFF 7.02 program [31] was used to calculate theoretical phase and amplitude functions of As–O, As–O–O multiple scattering, As–Al, As–Cu As–Fe, and As–Zn scattering paths using input files based on the structural refinement of adamite ($Zn_2[AsO_4]OH$), arthurite ($CuFe_2(OH)_2[AsO_4]_2{\cdot}4H_2O$), chalcophyllite ($Cu_9Al[AsO_4]_2[SO_4]_{1.5}(OH)_{12}{\cdot}18H_2O$), clinoclase ($Cu_3[AsO_4][OH]_3$), liroconite ($Cu_2Al[AsO_4](OH)_4{\cdot}4H_2O$), mansfieldite ($AlAsO_4{\cdot}2H_2O$), mapimite ($Zn_2Fe_3[AsO_4]_3(OH)_4{\cdot}10H_2O$), olivenite ($Cu_2[AsO_4]OH$, monoclinic), and scorodite ($FeAsO_4{\cdot}2H_2O$) [32–41].

2.4. Fitting procedure

The coordination numbers (N), radial distances (R), and a single cross-correlated E_0 shift (ΔE_0) for all shells were allowed to vary freely. The number of permissible free floating parameters ($N_{pts} = 2 \cdot \Delta k \cdot \Delta R/\pi$) for fits ranged between 4 and 6 depending on the range in $R + \Delta R$ [42]. The amplitude reduction factor (S_0^2) for all fits was fixed to 0.9. All fits were performed in a sequential manner adding scattering paths stepwise and recording reductions of the fit's residual, where applicable. Shells were added in order of distance from the central absorber as often as possible. The structural parameters of the best fits for mineral, precipitated and adsorbed phases on goethite and gibbsite are recorded in Tables 2, 3, and 4, respec-

Table 2
Structural parameters derived from non-linear least square fitting performed on Fourier-filtered (FF) second shells for As(V) bearing minerals and an Na_2HAsO_4(aq.) sample

	N[a]	R[b] (Å)	σ^2[c] (Å^2)	ΔE_0[d] (eV)	Res.[e]	Res. ↓[f] (%)		XRD N	XRD R (Å)	EXAFS accuracy N (±%)	EXAFS accuracy R (±Å^2)
Na_2HAsO_4(aq.)	FF-range = 2.00–2.80 Å, k^2										
MS[g]	9.3	3.06	<0.001	2.16	25.60						
Scorodite	FF-range = 2.50–3.30 Å, k^3						Scorodite				
As–Fe	4.6	3.33	0.006	2.09	25.11		As–Fe	4.0	3.36	13.0	0.030
Ojuelaite	FF-range = 2.20–2.90 Å, k^2						Ojuelaite				
MS	11.5	3.10	0.006	5.78	40.37		As–Fe	3.0	3.27		
As–Fe	1.3	2.93	0.008	5.78	19.7	51.2	As–Zn	1.0	3.33		
								4.0	3.28	47.8	0.005
	FF-range = 2.50–3.25 Å, k^3										
As–Fe/Zn	2.1	3.29	0.007	−3.64	21.4						
Chalcophyllite	FF-range = 2.50–3.40 Å, k^3						Chalcophyllite				
As–Cu	5.4	3.32	0.007	3.82	15.2		As–Cu	6.0	3.33	9.7	0.002
Olivenite	FF-range = 2.50–3.40 Å, k^3						m-Olivenite P2(1)/n				
As–Cu	5.5	3.26	0.006	−0.51	16.6		As–Cu	5.0	3.29	9	0.03
As–Cu	1.2	3.47	0.006	−0.51	16.1	3.0	As–Cu	3.0	3.43	60	0.04
										28.3	0.03
Adamite	FF-range = 2.50–3.50 Å, k^3						Adamite				
As–Zn	7.5	3.33	0.006	−0.57	17.0		As–Zn	8.0	3.34	6.5	0.011
	FF-range = 5.30–5.80 Å, k^3										
As–As	3.2	6.00	0.002	−1.87	31.2		As–As	4.0	6.04	20.5	0.040

[a] N = coordination number.
[b] R = radial distance.
[c] σ^2 = Debye–Waller parameter.
[d] ΔE_0 = phase shift.
[e] Res. = residual.
[f] Res. ↓ = the percent decrease of the residual as a result of adding that particular scattering path to the fit.
[g] MS = multiple (triple, O–O–As) scattering in the As(V, AsO_4) tetrahedron.

Table 3
Structural parameters derived from non-linear least square fitting performed on Fourier-filtered (FF) second shells for metal-arsenate precipitates in aqueous solution and in the presence of α-Cr_2O_3 and SiO_2

Homogeneous precipitates							Heterogeneous precipitates on α-Cr_2O_3						
	N[a]	R[b] (Å)	σ^2[c] (Å^2)	ΔE_0[d] (eV)	Res.[e]	Res. ↓[f] (%)		N	R (Å)	σ^2 (Å^2)	ΔE_0 (eV)	Res.	Res. ↓ (%)
AsCu	FF-range = 2.40–3.30 Å, k^3						AsCu	FF-range = 2.40–3.30 Å, k^3					
As–Cu	5.6	3.23	0.006	2.79	21.4		As–Cu	8.1	3.23	0.008	5.91	17.2	
As–Cu	2.4	3.39	0.006	2.79	15.3	28.7	As–Cu	3.2	3.42	0.008	5.91	13.5	21.7
AsCuZn	FF-range = 2.40–3.30 Å, k^3						AsCuZn	FF-range = 2.40–3.30 Å, k^3					
As–Cu	3.9	3.22	0.009	−2.41	18.9		As–Cu	4.19	3.21	0.007	0.01	16.6	
As–Zn/Cu	1.1	3.38	0.009	−2.41	16.6	12.1	As–Zn/Cu	1.1	3.39	0.007	0.01	14.6	12.4
AsZn	FF-range = 2.50–3.50 Å, k^3						AsZn	FF-range = 2.50–3.45 Å, k^3					
As–Zn	2.1	3.26	0.005	−0.04	34.7		As–Zn	1.7	3.24	0.004	0.24	28.5	
As–Zn	2.6	3.40	0.005	−0.38	22.8	34.3	As–Zn	2.4	3.38	0.004	0.24	21.9	23.4
							$AsZnSiO_2$	FF-range = 2.50–3.60 Å, k^3					
							As–Zn	2.3	3.25	0.003	1.52	46.5	
							As–Zn	2.7	3.39	0.003	1.52	23.0	50.5

[a] N = coordination number.
[b] R = radial distance.
[c] σ^2 = Debye–Waller parameter.
[d] ΔE_0 = phase shift.
[e] Res. = residual.
[f] Res. ↓ = the percent decrease of the residual as a result of adding that particular scattering path to the fit.

tively. The estimated accuracies for N and R were based on a comparison of our best fit results for the mineral species with values from refined XRD measurements published in the literature.

3. Results

3.1. Visual inspection of XANES and raw $\chi(k)$ spectra

XANES spectra and raw, k^3-weighted $\chi(k)$ (EXAFS) spectra of selected As(V)-containing solid phases and an aqueous Na_2HAsO_4 standard show that the discernible differences among adsorbed phases on gibbsite and goethite were few and minor (Figs. 1a and 1b). Conversely, precipitated and mineral phases had significantly more developed and differentiated absorption features in the XANES region and showed distinct beat nodes in their EXAFS spectra making a differentiation among these phases possible. Therefore, adsorbed phases could be differentiated from precipitated and mineralized species, however, among adsorbed phases, the strong contributions to the EXAFS signal from the first ligand shell made an unambiguous differentiation difficult.

3.2. k-range and k-weight dependencies

The shape and magnitude of the modulus and imaginary part in Fourier transforms depend on several factors including the k-range and k-weighting, and thus, several FTs of different k-weights and k-ranges should be examined in order to obtain a better understanding of the data [30]. Fourier transforms of aqueous, adsorbed and mineralized As(V) species were analyzed for their dependence on the selected k-range and k-weight (Figs. 2a–2i). For all FTs (Figs. 2a–2i), the lower r-space of the first shell between 0.8 and 1.8 Å (uncorrected for phase shift) had diminished amplitudes if a k-range of 3.5–12.75 Å^{-1} was Fourier transformed, but the peak position itself did not shift as a result of changing either the k-weight or k-range. Conversely, altering the k-range and the k-weight shifted and suppressed peaks in the second shell of the aqueous and the adsorbed As(V) species. The broad peak between 2.0 and 2.8 Å (uncorrected for phase shift) in the FT of Na_2HAsO_4(aq.) decreased with increasing k-weight and was suppressed if the k-range was increased from 2.5 to 3.5 Å^{-1} (Figs. 2a–2c). This behavior of the "second shell" was consistent with that of MS in CrO_4^{2-}(aq.) tetrahedra [18]. A similar dependence on k-range and k-space was observed for AsGoe_1mo (Figs. 2d–2f). With decreasing k-weight (3 to 1), the left-hand side shoulder of the broad second shell peak between 2.2 and 3.4 Å became better expressed if the k-range was maintained between 2.5 and 12.75 Å^{-1}. However, when decreasing the k-range to 3.5 Å^{-1}, the shoulder contributions were greatly diminished (Figs. 2d–2f). As this behavior was overall similar to that of the aqueous sample, in which only MS contributions were measured (and fitted), and was also observed in the mineral sample adamite (Figs. 3g–3i), it could be reasonably inferred that the broad second shell between 2.2 and 3.4 Å (uncorrected for phase shift) in Fig. 3f was partially composed of contributions from multiple scattering. To elucidate the contributions from MS by non-linear least-square fitting, the raw EXAFS data were k^2-weighted, Fourier transformed over a k-range of 2.5–12.75 Å^{-1} and Fourier filtered over r-space between 2.2 to 2.7 Å (see Tables 2, 3 and 4). To elucidate the contributions from higher order shells, the raw EXAFS data were k^3-weighted, Fourier transformed over a k-range of 2.5–12.75 Å^{-1} and Fourier filtered over r-space $\geqslant$2.5 Å.

Table 4
Structural parameters derived from non-linear least square fitting performed on Fourier-filtered (FF) second shells for As(V) sorption samples on gibbsite and goethite in the presence and absence of Cu(II) and or Zn(II)

	N[a]	R[b] (Å)	σ^2[c] (Å^2)	ΔE_0[d] (eV)	Res.[e]	Res. ↓[f] (%)		N	R (Å)	σ^2 (Å^2)	ΔE_0 (eV)	Res.	Res. ↓ (%)
AsGib_1d	FF-range = 2.20–2.70 Å, k^2						AsGoe_1d	FF-range = 2.20–2.70 Å, k^2					
MS[g]	18.0	3.11	0.003	5.7	28.7		MS	12.6	3.11	0.001	4.7	31.4	
As–Al	0.4	2.72	0.008	5.7	20.8	27.5	As–Fe	0.2	2.87	0.001	4.7	17.6	44.2
	FF range = 2.50–3.20 Å, k^3							FF range = 2.50–3.30 Å, k^3					
MS	4.61	2.90	0.002	8.12	13.1		As–Fe	1.7	3.28	0.005	0.1	32.3	
As–Al	1.6	3.17	0.004	8.1	13.1								
AsGib_aged	FF range = 2.20–2.70 Å, k^2						AsGoe_1mo	FF-range = 2.20–2.70 Å, k^2					
MS	18.7	3.11	0.005	5.9	20.9		MS	12.0	3.14	0.003	4.8	31.1	
As–Al	0.8	2.76	0.009	5.9	19.8	5.4	As–Fe	0.3	2.89	0.007	4.8	21.5	30.9
	FF range = 2.50–3.20 Å, k^3							FF-range = 2.50–3.30 Å, k^3					
MS	6.98	2.90	0.004	7.51	9.8		As–Fe	1.2	3.28	0.003	−2.7	20.8	
As–Al	2.776	3.17	0.006	7.51	9.8								
AsCuGib	FF range = 2.20–2.70 Å, k^2						AsCuGoe	FF-range = 2.20–2.70 Å, k^2					
MS	12.3	3.10	0.002	7.1	35.7		MS	12.1	3.11	0.004	6.7	32.4	
As–Cu	0.3	2.82	0.005	7.1	13.0	63.7	As–Cu/Fe	0.4	2.85	0.008	6.7	14.0	56.7
	FF range = 2.50–3.20 Å, k^3							FF-range = 2.50–3.40 Å, k^3					
As–Cu	1.6	3.23	0.008	−0.4	18.5		As–Cu/Fe	1.8	3.27	0.007	1.0	19.1	
AsZnGib	FF-range = 2.20–2.70 Å, k^2						AsZnGoe	FF-range = 2.20–2.70 Å, k^2					
MS	17.4	3.09	0.005	5.9	34.3		MS	13.4	3.13	0.004	5.1	32.3	
As–Al/Zn	0.8	2.75	0.010	5.9	20.4	40.5	As–Fe/Zn	0.4	2.86	0.008	5.1	26.6	17.7
	FF range = 2.50–3.15 Å, k^3							FF-range = 2.50–3.40 Å, k^3					
MS	4.9	2.88	0.003	5.8	14.5		As–Fe/Zn	2.1	3.29	0.007	−2.0	17.0	
As–Al/Zn	1.8	3.13	0.005	5.8	14.5								
AsCuZnGib	FF-range = 2.20–2.70 Å, k^2						AsCuZnGoe	FF-range = 2.20–2.70 Å, k^2					
MS	12.3	3.09	0.003	7.0	36.2		MS	10.9	3.11	0.003	6.7	34.5	
As–Cu	0.3	2.82	0.005	7.0	14.4	60.2	As–Fe/Cu/Zn	0.3	2.84	0.005	6.7	13.3	61.5
	FF-range = 2.50–3.30 Å, k^3							FF-range = 2.50–3.30 Å, k^3					
AsCu/Zn	1.6	3.25	0.008	0.9	22.1		As–Fe/Zn	1.6	3.28	0.009	1.1	25.8	

[a] N = coordination number.
[b] R = radial distance.
[c] σ^2 = Debye–Waller parameter.
[d] ΔE_0 = phase shift.
[e] Res. = residual.
[f] Res. ↓ = the percent decrease of the residual as a result of adding that particular scattering path to the fit.
[g] MS = multiple (triple, O–O–As) scattering in the As(V, AsO_4) tetrahedron.

3.3. Minerals and precipitates

Structural parameters for second shell fits of As(V) bearing minerals indicated an accuracy for N and R in the second shell of ±19% and ±0.03 Å, respectively (Table 2). The accuracy of N ranged between 8 and 33% (adamite and ojuelaite, respectively) and for R between 0.01 and 0.05 Å (adamite and scorodite, respectively). The average Debye–Waller parameter (σ^2) was 0.006 ± 0.002 Å^2. The average distance between As and neighboring metal atoms in the mineralized species was 3.34 Å. The different coordination environments of As(V) beyond the first shell were well differentiated based on Fourier filtered second shell peaks in radial structure functions. Phase shifts and differences in the absorption envelopes (incl. amplitudes) permitted differentiation among copper-arsenate minerals and precipitates (Fig. 3a), among different As(V) bearing minerals (adamite, scorodite and olivenite, Fig. 3b), and among zinc-arsenate minerals and precipitates (Fig. 3c). These differences are related to the number of backscattering neighbor(s) and their atomic number (Z) as well as the different crystal structures in which As(V) is incorporated. For example, the Fourier-filtered contributions of second shell Cu atoms of chalcophyllite, olivenite (monoclinic-β) and the homogeneous copper-arsenate precipitate (CuAsPrecip) were well out of phase reflecting the fitted results that Cu atoms occurred at a greater average distance from As(V) in chalcophyllite than in olivenite than in the CuAsPrecip (Fig. 3a). Despite the lack of a phase shift, the absorption envelopes of adamite and the homogeneous zinc-arsenate precipitate (ZnAsPrecip) differed substantially in amplitude as well as in distribution with the ZnAsPrecip having a broad beatnode occurring between 10 and 12 Å^{-1} that reflected second shell Zn neighbours at ca. 3.29 and 3.42 Å.

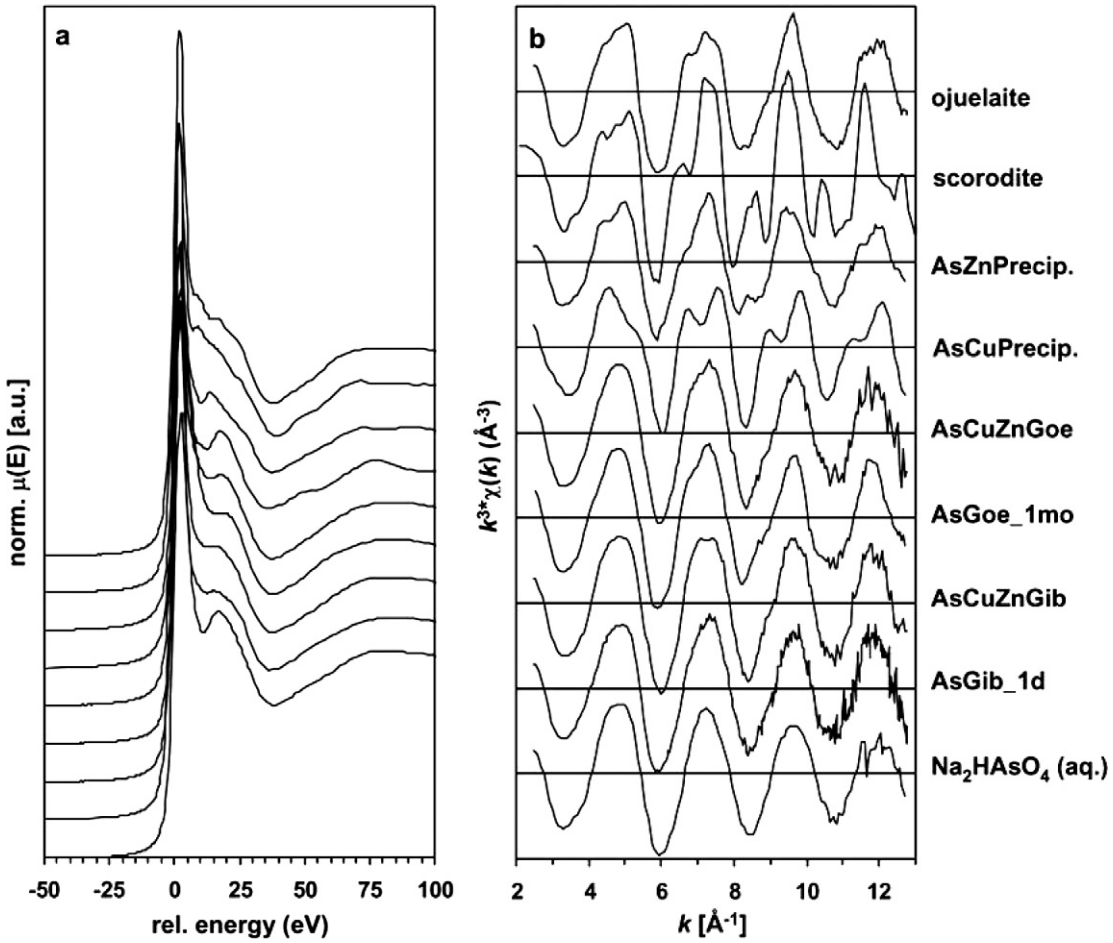

Fig. 1. (a) XANES and (b) raw k^3-weighted $\chi(k)$ As(V) spectra of selected aqueous, adsorbed, precipitated and mineralized species. The relative energy 0 was set to 11.874 eV. A differentiation of sorption states is possible only between precipitated phases with different structure and precipitates from aqueous and or adsorbed phases.

Homogeneously and heterogeneously derived precipitates of As(V) and Cu(II) ions produced quasi-isostructural precipitates in which the average bonding environment of As(V) was controlled by ca. 6 Cu atoms at 3.21 Å broadly consistent with the structure of clinoclase (Table 3). The significantly shorter As–Cu distance shifted the wavefunction of CuAsPrecip to higher k-values when directly compared to ZnAsPrecip permitting differentiation among the zinc-arsenate and copper-arsenate species (Fig. 3d). A slight shift in phase of wavefunctions of AsCu and AsCuZn complexes precipitated in the presence of α-Cr_2O_3 were also observed, which may suggest that As(V) was partly coordinated by eskolaite's surface (Figs. 3e and 3f). The As–Cr distance is ca. 3.25 Å [43] and is similar to that of As–Cu in the clinoclase and monoclinic olivenite structures [36,37]. In the presence of Zn, the number of Cu neighbours at 3.21 Å decreased by ca. 50%, but additional ($N \sim 3$) contributions from either Zn and or Cu atoms occurred at ca. 3.39 Å (Table 3). The greater number of metal neighbors at ca. 3.39 Å was to some extent apparent from the greater asymmetry of the second shell peak of the mixed precipitates vs those of the pure CuAs precipitates (figure not shown). In the presence of α-Cr_2O_3 and SiO_2, Zn atoms occurred at ca. 3.25 and 3.44 Å, which most closely resembled the distribution of Zn atoms around AsO_4 in the koettigite structure (Fig. 3g).

3.4. Gibbsite and goethite

Figs. 4a–4h provide a comprehensive overview and comparison of Fourier transforms and Fourier filtered second shell contributions of As(V) sorption samples on goethite and gibbsite. In the absence of Cu and Zn, the modulus magnitude of AsGib_1d was smaller than that of AsGoe_1d (Fig. 4a), which is in good agreement with Al being a weaker backscattering neighbor than Fe due to the lower atomic number of Al ($Z_{Al} = 13$ vs $Z_{Fe} = 26$). Consequently, the Fourier filtered $\chi(k)$ contributions from second shell Al neighbors had a significantly lower amplitude than contributions from second shell Fe neighbors (Fig. 4b). In addition to that, the absorption envelope of the two wavefunctions differed significantly from each other. Interestingly, the phase shift between the two spectra is limited and only apparent at low k values, despite best fitting results suggesting a difference in distance between second shell neighbors of ca. 0.11 Å. The lack of a phase shift between the wavefunctions may be related to phase shift differences (ΔE_0) measured for AsGib_1d during non-linear least-square fitting (Table 4), which (i.e., the phase shift) affects the phase of the wavefunction in a similar way as the interatomic distance (R) does [44]. Conversely, As–Al contributions at 3.16 Å may also be the result of two As–Al distances, one at 3.30 Å and one at 3.05 Å,

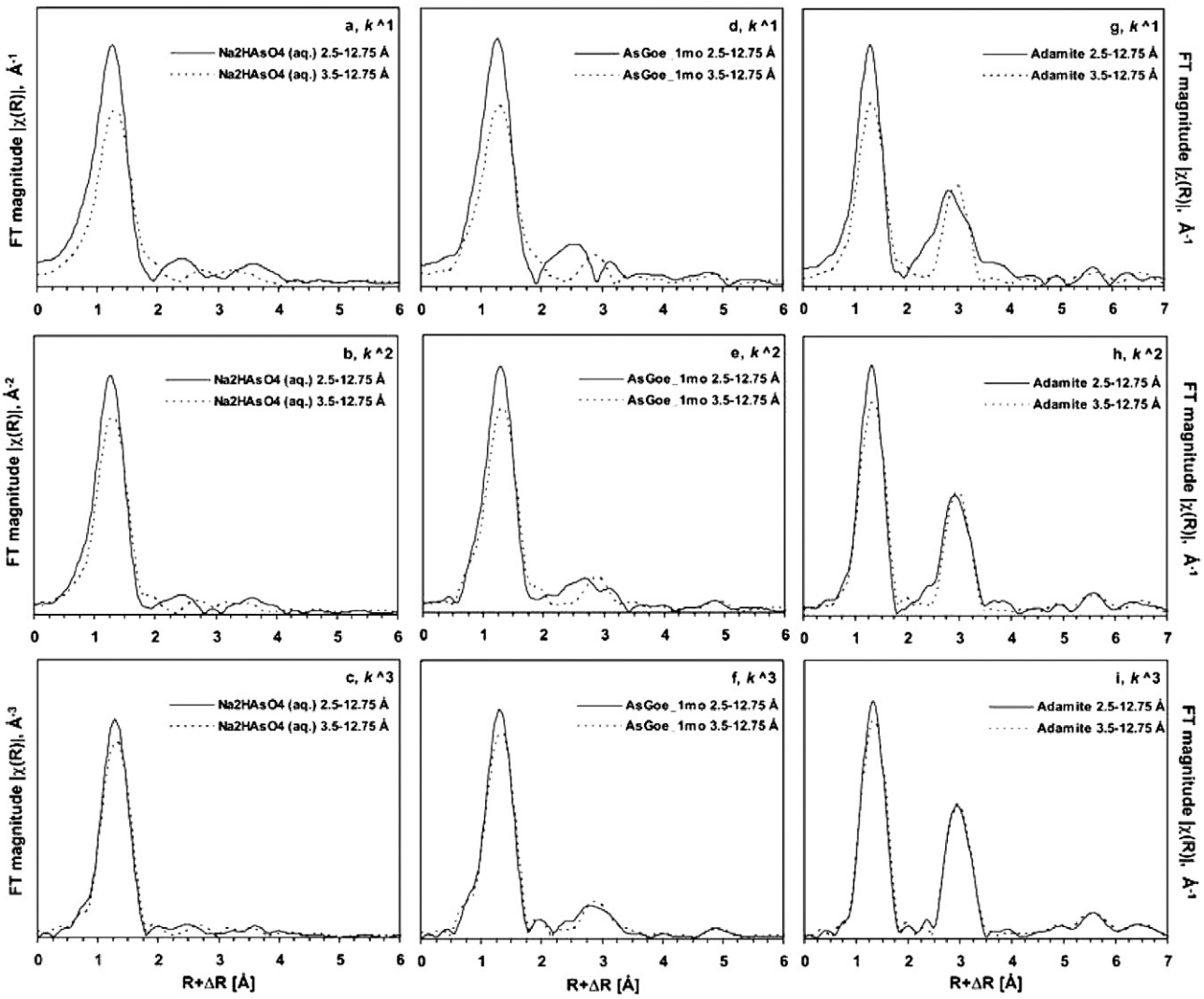

Fig. 2. Dependence of first and second shells in Fourier transforms on k-weight and k-range for three selected As-bearing phases: (a–c) Na_2HAsO_4(aq.) representative of outer-sphere species and thus absence of a second shell; (d–f) As(V) equilibrated on goethite for one month representative of a typical surface adsorbed species; and (g–i) adamite representative of a three dimensionally coordinated species. The dynamics of the peak between 2.2 and 2.8 Å (uncorrected for phase shifts) as a function of k-weight and k-range demonstrate the existence of multiple scattering (MS) contributions in the raw EXAFS function across all sorption states (outer-sphere, surface adsorbed inner-sphere complex and precipitated/mineralized form).

which would converge towards 3.15 Å when fitting with a single As–Al scattering path. In the presence of Cu, the Fourier transforms of AsCuGoe and AsCuGib appeared nearly identical (Fig. 4c). The wavefunction of AsCuGoe however was shifted to lower k values, which was consistent with the greater average distance between As(V) and the second shell neighbor in the goethite-based sample (Fig. 4d). Furthermore, we noticed that ΔE_0 values of the AsCuGib and the AsCuGoe sample were quite similar (−0.4 vs 1.0), which suggested that (a) the phase shift between the two wavefunctions could be related to the discrepancy in inter-atomic distance between the second nearest neighbors and (b) the second nearest neighbor in the AsCuGib sample was unlikely to be Al, and rather Cu, since in the absence of Cu and Zn, ΔE_0 was $\geqslant$7.5 (Table 4). Similar ΔE_0 values, Fourier transforms and Fourier filtered second shell contributions were observed when comparing CuZnAsGoe with CuZnAsGib (Figs. 4e and 4f). The significance of Cu(II) in the bonding environment of As(V) became more evident when only Zn was allowed to react with As(V) at the surfaces. Despite the discrepancies between Fourier transforms, the Fourier-filtered second shell wavefunctions were well in phase up to ca. 9 $Å^{-1}$, despite the inter-atomic distances between As and the second shell neighbor differing by 0.16 Å (Figs. 4g and 4h). The slight shift of the AsZnGoe wavefunction to lower wavenumbers and the wavelength contraction was consistent with the expected frequency increase of the wavefunction stemming from second shell Fe/Zn neighbors occurring at a greater distance from As than Al neighbors.

The Fourier transforms of As(V) sorption samples on goethite and gibbsite showed consistent low amplitude second shell features for all samples, suggesting that As(V) did not form precipitates on goethite or gibbsite in the presence of Cu and or Zn consistent with the fit results which showed N (coordination number) to be between one and two (Figs. 5a and 6a,

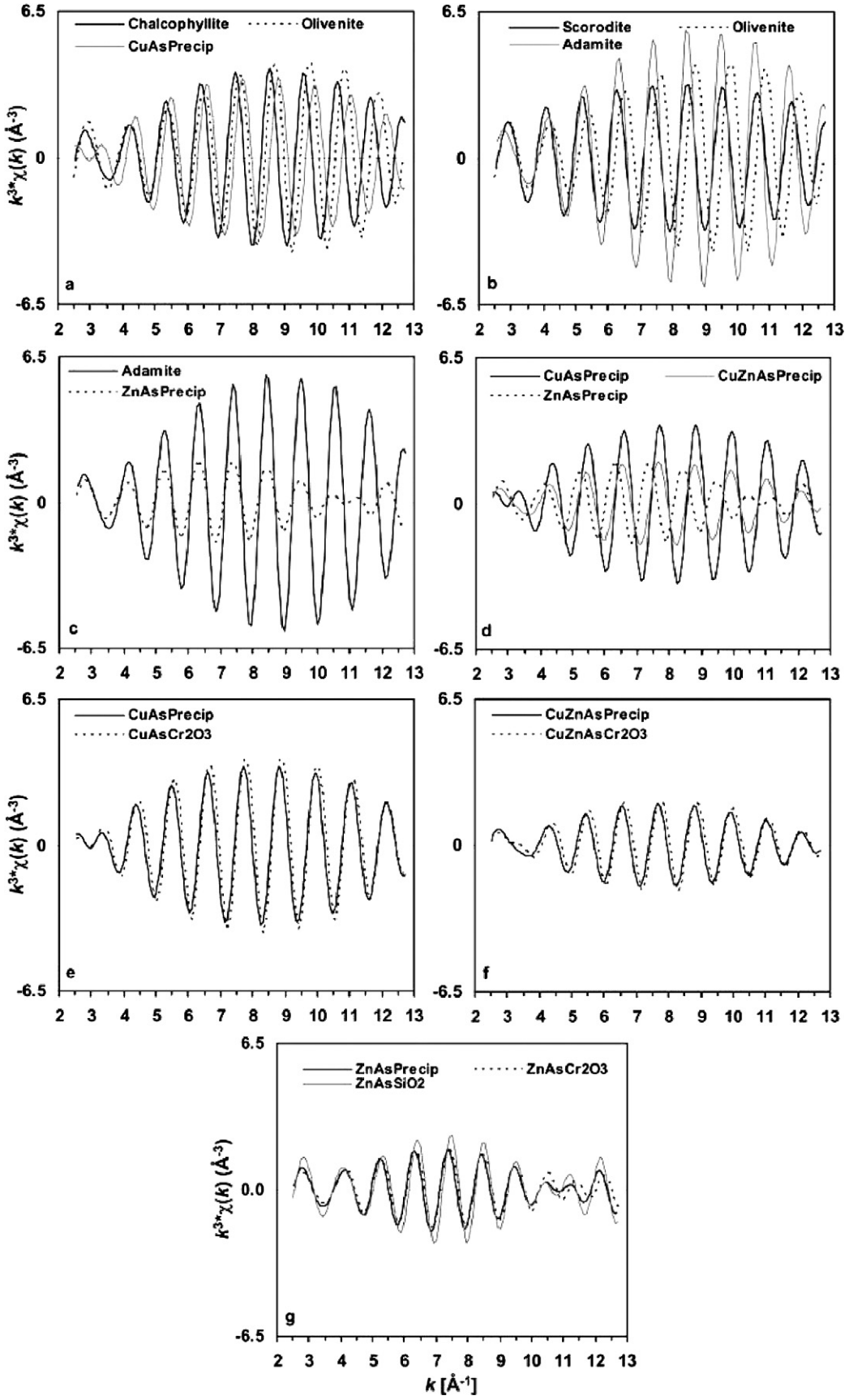

Fig. 3. Comparison of Fourier-filtered second and third shells of selected As(V)-bearing minerals and precipitates. Phase shifts and amplitude discrepancies reflect differences in the coordination environment and type of second and third nearest atomic neighbors.

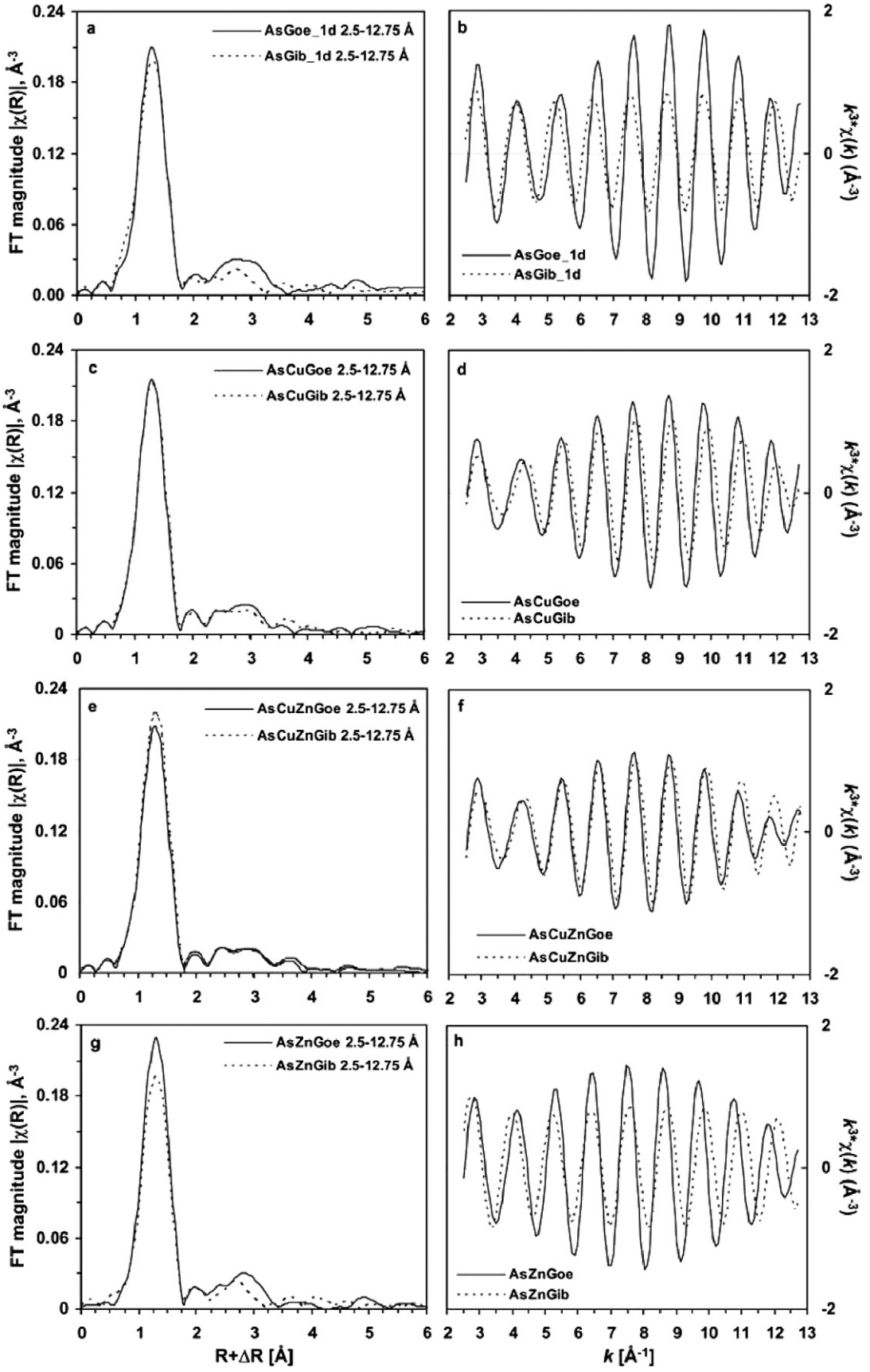

Fig. 4. Direct comparison of Fourier transforms and Fourier-filtered second shells of As(V) sorbed on goethite vs gibbsite in the presence of Cu(II) and or Zn(II). Differences in absorption envelopes and phase shifts aid in the differentiation of likely and less likely second nearest neighbors. The close similarity of FTs of sample containing Cu suggests that As(V) is partly bonding via Cu on both goethite and gibbsite.

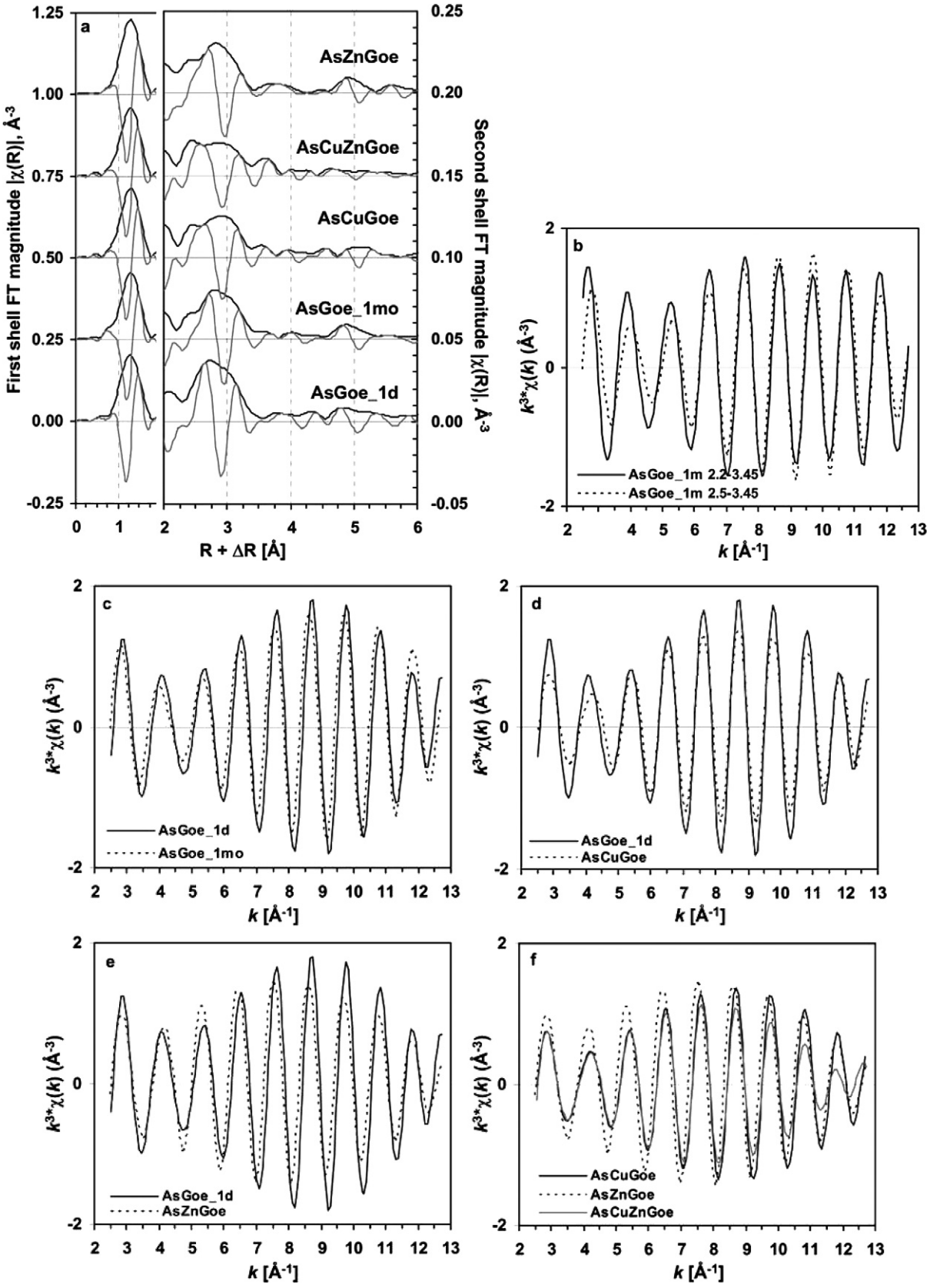

Fig. 5. (a) Fourier transforms of As(V) sorbed on goethite in the presence and absence of Cu(II) and or Zn(II). The FT magnitude of the first shell is on the left ordinate axis, while the FT magnitude of the second and third shells is on the right ordinate axis. The modulus of the FTs is represented by the solid black lines, while the imaginary part is represented by the grey lines. (b) Effect of r-range (2.2 vs 2.5 to 3.45 Å) on beatnodes in the Fourier-filtered wavefunctions. (c and d) Direct comparison of the Fourier-filtered contributions from r-space between 2.5 and up to 3.45 Å (see Table 4). The lack of phase shifts and differences in the absorption envelopes suggest that complimentary Cu and Zn K-edge EXAFS data are necessary to identify if As(V) is binding directly with Cu and or Zn.

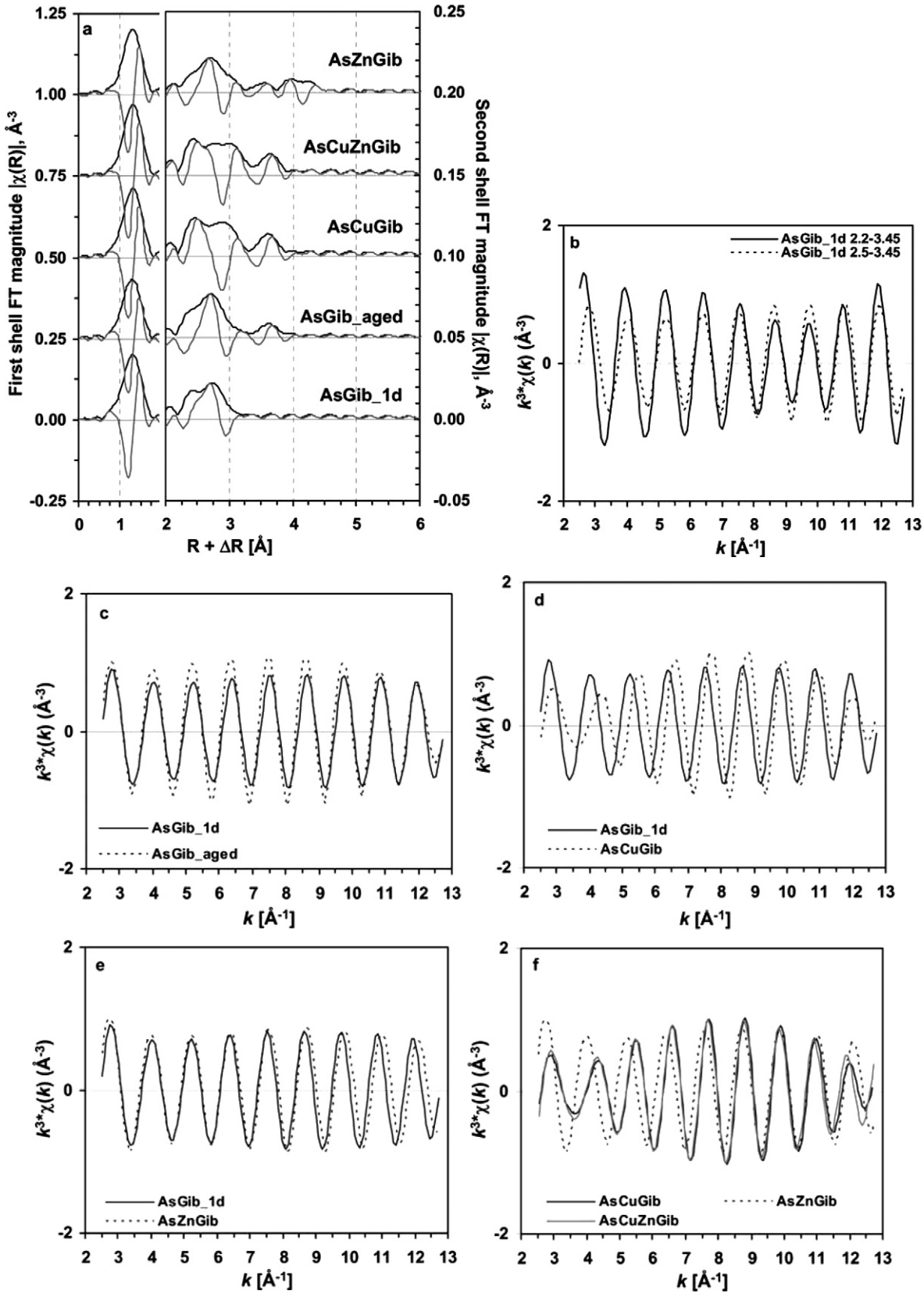

Fig. 6. (a) Fourier transforms of As(V) sorbed on gibbsite in the presence and absence of Cu(II) and or Zn(II). The FT magnitude of the first shell is on the left ordinate axis, while the FT magnitude of the second and third shells is on the right ordinate axis. The modulus of the RSFs is represented by the solid black lines, while the imaginary part is represented by the grey lines. (b) Effect of r-range (2.2 vs 2.5 to 3.45 Å) on beatnodes in the Fourier-filtered wavefunctions. (c and d) Direct comparison of the Fourier-filtered contributions from r-space between 2.5 and up to 3.30 Å (see Table 4). Phase shifts and differences in the absorption envelopes suggest that Cu(II), but not Zn(II) is coordinating As(V) at the gibbsite–water interface.

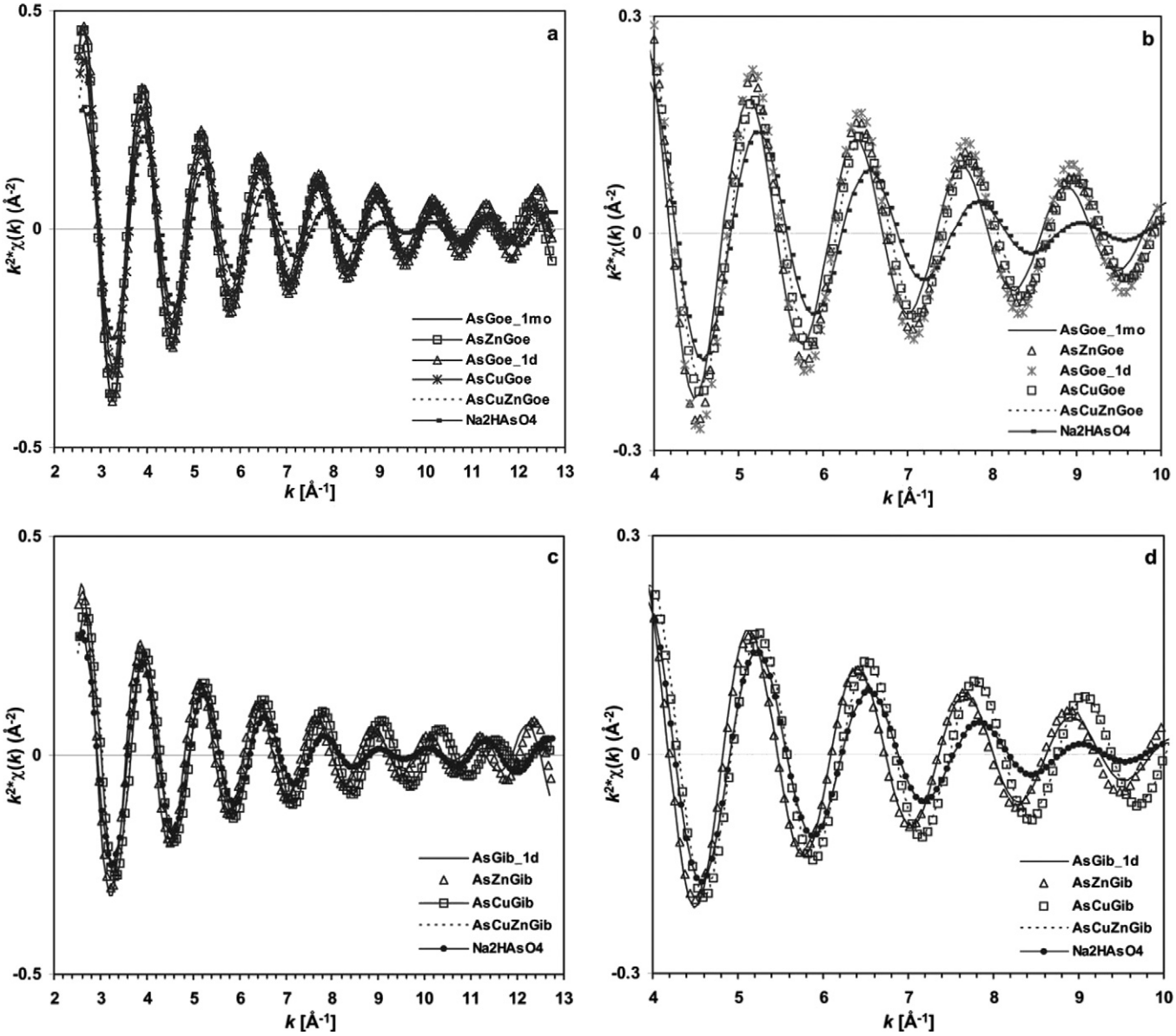

Fig. 7. Direct comparison of Fourier-filtered contributions from r-space between 2.2 and 2.7 Å of As(V) adsorption complexes on goethite (a and b) and gibbsite (c and d) with Na_2HAsO_4(aq.). With increasing k-space, the amplitude of the Na_2HAsO_4(aq.) wavefunction diminishes relative to the adsorbed phases and is increasingly out of phase, which suggests the presence of another backscattering neighbor, which can be fitted with Al and Fe neighbors at distances characteristic of an edge-sharing complex. Hereby it is noteworthy that the edge-sharing distance of As(V) to Al is significantly shorter than to Fe allowing a distinction of next nearest neighbors for this surface complex.

Table 4). The broad second shell feature of the As(V) RSF (2.20–3.40 Å $R + \Delta R$) pointed toward multiple backscattering neighbors contributing to the EXAFS signal. Modulations of the Fourier filtered second shell as a function of the range in r-space showed two beatnodes at high ($\sim$10 Å^{-1}) and low (4–5 Å^{-1}) k values (Figs. 6b and 7b). The beatnode at low k occurred if the lower end of the r-range started at ca. 2.5 Å. This beatnode reflected contributions from multiple scattering in the tetrahedral structure of AsO_4 (O–O–As) consistent with our findings above concerning differential k-weighting and k-ranging (Fig. 2). The beatnode at high k occurred only if the r-range was decreased below 2.5 Å. This beatnode could hence reflect the interference of the backscattering waves of the ^{1}E and ^{2}C complexes as advocated previously, because the ^{1}E complex (ca. 2.70 Å) occurs presumably at a shorter distance than MS contributions (ca. 3.10 Å) [16]. A possible ^{1}E surface complex and contributions from MS thus appeared to be the main components of the prominent left-hand shoulder, which was observed in most of our samples. In the presence of Cu, this shoulder feature had a similar amplitude as the main shell feature and in samples on gibbsite, the presence of Cu caused a distinct shift in the imaginary part [*vide infra*]. The ^{2}C surface complexes were isolated from MS and potential ^{1}E contributions by k^3-weighting the raw EXAFS data and Fourier transforming from 3.5 to 12.75 Å^{-1}. This worked well for As(V) spectra from goethite-based samples, because the ampli-

tude function of the As–Fe scattering path is not influenced by the reduction in the k-range. Conversely, the amplitude function of the As–Al scattering path was significantly reduced if the k-range was reduced from 2.5 to 3.5 $Å^{-1}$ thus compromising the data quality of the gibbsite-based As(V) samples. In Figs. 5c–5f and 6c–6f, the beatnode from MS contributions at low k-values was still apparent, because the raw EXAFS functions were Fourier transformed from 2.5 to 12.75 Å and Fourier-filtered from 2.5 Å $R + \Delta R$ in order to cross-compare the Fourier filtered shells of As(V) among sorbents (Figs. 4a–4h). Among spectra for As(V) samples sorbed on goethite, the fitting results did not suggest that there were measurable differences among the samples. Small phase shifts were noticeable between AsZnGoe and AsGoe_1d and AsCuGoe (Figs. 5e and 5f), however, the AsZnGoe sample was well in phase with the AsGoe_1mo sample. The wavefunctions of Fourier-filtered second shells of As(V) sorbed on gibbsite were largely in phase with each other (Figs. 7b–7d) with the exception of AsCuGib and AsCuZnGib. These phase shifts were corroborated by the fit results, which showed that the average inter-atomic distance between As(V) and its primary second shell was ca. 3.25 Å for Cu containing samples and ca. 3.15 Å for non-copper containing samples including those containing Zn(II). In addition, and as mentioned earlier, Cu(II) containing samples exhibited significantly lower ΔE_0 values than in the absence of Cu(II). Therefore, Cu atoms may be differentiated from Al atoms in the second shell of As(V).

Multiple scattering and potential ^{1}E complexes were isolated from ^{2}C complexes by k^2-weighting, Fourier transforming the raw EXAFS function between 2.5 to 12.75 $Å^{-1}$, and Fourier filtering the resulting peaks in the FT between 2.2 and 2.7 Å (uncorrected for phase shifts). The ^{2}C complex became apparent by an increase in the amplitude of the Fourier-filtered wavefunction at high k if the range in r-space was increased above 2.7 Å. The Fourier-filtered shells (2.2 to 2.7 Å $R + \Delta R$) of Na_2HAsO_4(aq.) and the adsorbed As(V) samples differed in two main aspects (Figs. 7a and 7b): (1) The wavefunctions of adsorbed samples were shifted to lower k values than the wavefunction of Na_2HAsO_4(aq.) and also had higher frequencies; and (2) the amplitude of the wavefunction of adsorbed samples had a greater amplitude above 7 $Å^{-1}$. The phase shift can be related back to the greater R_{MS} for most of the adsorbed samples, the amplitude discrepancy however suggested contributions from a backscattering neighbor. The fit results for these spectra showed that the inclusion of the second fitting path (As–Fe/Al/Cu/Zn) improved the fit by an average of $40 \pm 20\%$, ranging between ca. 5 and 65%. The fit results showed furthermore that the position of this shell was dependent on the adsorbent, i.e., goethite or gibbsite, and the presence of a foreign metal, specifically Cu(II). Our best fit results showed that the $^1E_{As–Al}$ complex (ca. 2.74 Å) is ca. 0.1 Å shorter than the $^1E_{As–Fe}$ complex (ca. 2.86 Å). Interestingly, the presence of Cu in gibbsite-based samples caused the $^1E_{As–M}$ to shift to 2.82 Å, which was similar to the distance we obtained for As(V) sorption samples on goethite in the presence of Cu(II, 2.85 Å). This could suggest that Cu is capable of complexing As(V) via a corner-(^{2}C) as well as an edge-sharing complex (^{1}E). This distinction by Cu(II) was also apparent from Figs. 7c–7d. The wavefunctions of AsCuGib and AsCuZnGib were distinctly out of phase with the other As(V) sorption samples on gibbsite. Among the goethite-based samples, however, there was no distinct phase shift among the samples other than to the Na_2HAsO_4(aq.) standard.

4. Discussion

4.1. Homogeneous and heterogeneous precipitates

In the presence of Cu(II) and Zn(II), Cu(II) induced the formation of Cu-arsenate structures (e.g., clinoclase). The presence of Zn(II) reduced the number of Cu neighbors by ~50% suggesting that Zn possibly interfered in their formation rather being incorporated. This more aggressive behavior by Cu(II) is consistent with Cu(II)'s greater thermodynamic stability with As(V) and its ability to polymerize in solution under neutral to alkaline pH [pH 7: $\log IAP/K_{so}$, $Zn_3(AsO_4)_2{\cdot}5H_2O = 5.54$ vs $\log IAP/K_{so}$, $Cu_3(AsO_4)_2{\cdot}2H_2O = 10.11$; for initial concentrations of 10 mM As(V), 10 mM Cu(II) or Zn(II)]. Zn K-edge EXAFS, however, will be required to determine the true coordination environment of Zn(II) in precipitates that have adopted copper-arsenate like precipitate structures. Silica induced the formation of a koettigite-like precipitate despite initial As(V) and Zn(II) concentrations not exceeding 500 μM [$\log IAP/K_{so}$, $Zn_3(AsO_4)_2{\cdot}5H_2O = 0.365$]. In contrast, 750 μM of As(V) and Zn(II), As(V) and Cu(II) or As(V), Cu(II) and Zn(II) in the presence of gibbsite or goethite did not form precipitates suggesting that surfaces that have greater hydration promote surface adsorption reactions at the expense of precipitates [pH 7, $\log IAP/K_{so}$, $Zn_3(AsO_4)_2{\cdot}5H_2O = 1.16$; $\log IAP/K_{so}$, $Cu_3(AsO_4)_2{\cdot}2H_2O = 7.15$]. A similar observation was made for three different suspension concentrations of goethite (10, 100 and 1000 mg goethite L^{-1}) in the presence of 250 μM As(V) and Zn(II) [20]. Goethite concentrations of 10 and 100 mg L^{-1} supported the formation of zinc-arsenate precipitates after 24 and 72 h, respectively, whereas in 1000 mg L^{-1} suspensions no precipitates formed. It should be noted that at pH 7 and 750 μM Cu(II), both $Cu(OH)_2$ and tenorite (CuO) were supersaturated, which would help to explain the noticeable complexation of As(V) with Cu(II) in gibbsite suspensions.

4.2. Goethite and gibbsite

Acicular goethite-crystals, such as the ones used in this study, grow along the crystallographic c-axis (orthorhombic space group Pnmb) and terminate in {021} and {110} faces. With respect to surface adsorption reactions, the {021} and {110} faces determine the type and density of hydroxyl (OH) functional groups at the surface [45]. Likewise, gibbsite (monoclinic space group P 1 21/c 1) particles exhibit their greatest reactivity at the {100} and {010} faces where the valences of the exposed, singly-coordinated OH functional groups are not satisfied [46]. Infrared spectroscopy of deuterium-substituted goethite samples reacted with As(V) showed that As(V) bonded

preferentially with singly-coordinated (A-type) OH functional groups and secondly with triply-coordinated (B-type) OH functional groups [47]. Although there are many exposed A-type OH functional groups along the crystallographic *c*-axis of goethite (due to edge-sharing Fe-octahedra), there was no indication that these OH functional groups were utilized for bonding by AsO_4. In adamite for example, neighboring AsO_4 moeities arrange along the *c*-axis and occur at regular intervals of 6 Å. On goethite, there were no indications of neighboring As(V) groups every 6 Å. This would suggest that As(V) bonding along the *c*-axis of goethite at singly-coordinated O sites was at best irregular. The reason for not bonding at these exposed OH functional groups may be related to the inter-atomic OH functional group distance, which along the *c*-axis of goethite is ca. 3.01 Å, but along the *c*-axis of adamite is only 2.77 Å. The inter-atomic distances of neighboring OH functional groups on the surface of goethite and gibbsite may regulate (to some extent) the ability of AsO_4 to bond to the mineral surface, because AsO_4, as an oxyanion in (rigid) tetrahedral configuration, is limited in its ability to increase or decrease the O–As–O angle and thus its own capacity to spread its O appendages apart (ideally ca. 2.74 Å based on R_{MS} of the Na_2HAsO_4(aq.) sample). On goethite's {110} and {021} faces, inter-atomic OH distances range from 2.89 to 2.93 Å and involve OH functional groups stemming from edge-sharing ($R_{Fe–Fe} = 3.29$ Å) and vertex-sharing ($R_{Fe–Fe} = 3.43$ Å) Fe-octahedra. On gibbsite, the inter-atomic OH functional group distance ranges from 3.00 to 3.45 Å and involves OH functional groups stemming from edge-sharing Al-octahedra ($R_{Al–Al} =$ 2.88–2.95 Å) except for one case in which the inter-atomic OH functional group distance is 3.05 Å occurring at the narrowest point across the distorted hexagonal cavity of gibbsite. The larger inter-atomic OH distances would explain why the inter-atomic As–Al distance of the ^{2}C surface complexes in gibbsite-based samples is shorter than the As–Fe distance in goethite-based samples. In comparison, AsO_4 bearing minerals (mapimite, adamite or mansfieldite) exhibit inter-atomic distances between OH functional groups of 2.62 (mansfieldite) to 2.83 Å (mapimite, ^{2}C complex).

Interestingly, the distance between two OH functional groups coordinated by the same Fe/Al octahedron (effectively the polyhedral edge distance) on goethite ranges from 2.56 to 2.93 Å and on gibbsite from 2.71 to 2.87 Å. Here again, the longer average OH edge distance in gibbsite-based samples would imply that a possible As–Al edge-sharing surface complex would be shorter than its As–Fe counterpart on goethite as was observed in this study. Based on density functional theory (DFT), recent studies [12,17] reported that As–Fe/Al edge-sharing complexes were energetically unfavorable in comparison to the ^{2}C complex and thus would either not form at all or only on specific surfaces (e.g., {021, 110} for goethite). The results of these studies must however be viewed critically. The $Al_2/Fe_2(OH)_2(H_2O)_8$ clusters used in the modeling were too simple and did not accurately reflect the complex geometries of the reactive surfaces of goethite or gibbsite nor the limitations imposed by a bulk structure. The two edge-sharing Al/Fe octahedra were not constrained by edge-sharing and/or corner-sharing to the bulk structure, which permitted the two singly coordinated OH functional groups to move closer to each other when constrained with an adsorbing AsO_4 moiety. While the results are internally consistent and accurate, they contradict EXAFS data collected by Manceau [16], Waychunas et al. [10,27] and this study. Sherman and Randall [17] fitted their raw EXAFS data in which the contributions of the second shell atoms (incl. MS) are obscured by the dominant contributions from single As–O scattering. Although edge-sharing complexes may contribute only minimally to the EXAFS signal, these surface complexes may be the most environmentally relevant ones. Three, the same authors did not attempt to determine the contributors to the broad second shell features otherwise they would have noticed that the shape and phase of the Fourier filtered $k^3 \cdot \chi(k)$ function varies according to the chosen range in *r*-space. Four, Ladeira et al. [12] interpreted their EXAFS data for a *k*-range between 3.9 and 14 Å, which not only removed contributions from MS but also significant contributions from backscattering Al atoms. Based on the careful analyses of the second shell peaks in the FTs of this study, the second shell of As(V) sorbed on goethite and gibbsite is a mixture of the surface complexes ^{1}E and ^{2}C and contributions from As–O–O–As multiple scattering.

4.3. Influences from Cu and Zn

Metal cations such as Cu(II) and Zn(II) form edge-sharing (Zn(II) on goethite) and corner-sharing complexes (Cu(II) on goethite) with the same OH functional groups on the reactive surfaces of goethite and gibbsite [48,49]. In addition, Cu(II) is known to form dimeric $[Cu_2(OH)_2(H_2O)_8]$ and other polymeric species at neutral to alkaline pH [50,51]. Metal surface complexes potentially limit access to vertices on Al/Fe-octahedra for AsO_4 sorption, however, at the same time may create a host of new, (likely) stronlgy hydrated OH functional groups. From As K-edge EXAFS data compiled in this study, second nearest Cu(II) and Zn(II) neighbors could not be ascertained unambiguously for goethite-based samples, however, the influence of Cu(II) on the second shell coordination environment of As(V) in gibbsite-based samples was apparent by the phase and amplitude shifts of the CuAsGib sample in comparison to the AsGib_1d/aged samples (Figs. 6d and 7b). The observed phase and amplitude shifts were likely due to AsO_4 bonding with polymeric Cu species at the gibbsite surface to form ^{2}C complexes as Zn(II) not have the same effect as Cu(II) did in the gibbsite-based samples despite similar ionic radii for Zn(II) and Cu(II) in octahedral coordination [52]. Polymeric Cu-species may likewise be responsible for the apparent sorption of As(V) as an edge-sharing complex. In a recent publication we showed that ca. 1 As atom can be fit at 3.33 Å in EXAFS data collected at the Zn K-edge [26]. Additional Cu and Zn K-edge EXAFS data would therefore be beneficial to ascertain the coordination environments of Cu(II) and Zn(II) at the goethite- and gibbsite-water interface in the presence of As(V). Such studies are however limited by the availability of beamtime at a hard X-ray beamline with suitable detectors.

With respect to the interpretation of As K-edge EXAFS data collected from heterogeneous soil and sediment samples, the

data reduction steps presented in this study suggest that raw, k^3-weighted EXAFS data were useful in separating precipitates from surface adsorbed species, but showed insufficient detail to separate among adsorbed species, including aqueous species. Fourier transforms provided additional insight to separate precipitates from surface adsorbed species and furthermore showed clear differences between specifically sorbed and outer-sphere surface complexes. To differentiate among adsorbed species, it was necessary to resolve the broad second shell features of the FTs. We suggest that following Fourier transformation of a k^2-weighted EXAFS function, a lower r-space window between 2.2 and 2.7 Å be Fourier-filtered for evaluation of the MS/^{1}E complexes. Given the significant phase shift between the Na_2HAsO_4(aq.) and surface adsorbed samples, outer-sphere and inner-sphere sorbed AsO_4 species could be evaluated. To evaluate second shell neighbors above 2.7 Å, it is feasible to move the lower end of the raw EXAFS k-range from 2.5 to 3.5 Å for Fourier transformation in order to minimize contributions to the RSF from MS. This will improve the resolution of the second shell at or above 2.8 Å (uncorrected for phase shifts). Figs. 6 and 7 show that upon Fourier filtering of the second shell, amplitude and phase shifts between spectra could be used to identify the more likely second shell neighbor(s).

5. Summary and conclusions

Arsenic K-edge EXAFS data were dominated by contributions from the first ligand shell (O) which mask low-amplitude contributions of higher frequency from second and third order shells as well as multiple scattering. To determine the nature of higher order shells it was necessary to carefully resolve all contributing elements: MS and ^{2}C (bidentate binuclear) and ^{1}E (bidentate mononuclear) surface complexes. The broad second shell of As(V) adsorbed on gibbsite or goethite consisted (in order of proximity to the central atom) of ^{1}E, MS and ^{2}C complexes. Non-linear least-square fitting of the Fourier-filtered r-range (2.2 to 2.7 Å) showed that MS matched the data in phase and amplitude up to ca. 6.75 Å^{-1}, but the total amplitude of the wavefunction was greater than the fitted MS contribution above 6.75 Å^{-1} in addition to being out of phase. Such behavior is consistent with a contribution from a lower-lying shell [44]. Based on our fit results, we propose that these contributions originate from bidentate mononuclear As(V) surface complexes on goethite and gibbsite ca. 2.85 and 2.70 Å away from the central atom, respectively. The surface stability of the ^{1}E complex under different environmental conditions and thus its environmental significance have to date not been established [5]. The specific contributions (Al vs Fe vs Cu vs Zn) to the EXAFS stemming from ^{2}C surface complexes could only be established for certain cases. Generally, $^2C_{As–Al}$ surface complexes could be differentiated from $^2C_{As–Fe}$ complexes based on differences in the absorption envelope as phase and amplitude shifts of the Fourier-filtered wavefunction. On goethite, neither Cu(II) nor Zn(II) influenced the wavefunction sufficiently as to infer bonding via Zn–OH or Cu–OH vertices. Zinc and Cu K-edge EXAFS are required to fully identify the surface complexes. On gibbsite, Zn(II) did not appear to contribute to the second shell bonding environment of As(V). This was apparent from a lack of phase and amplitude shifts in the Fourier filtered wavefunction as would be expected for Zn ($Z_{Zn} = 30$ vs $Z_{Al} = 13$). Conversely, Cu(II) caused phase and amplitude shifts of the Fourier-filtered wavefunction, which may be indicative of Cu(II) polymers binding AsO_4. The significance of the findings presented in this study is the ability of differentiating next nearest metallic cation neighbors on the basis of their photo-electron scattering properties with As(V), which enables the identification of the more likely next nearest atomic neighbours to As(V) in contaminated environments through linear fitting.

Future research should focus on evaluating the stability of As(V), Cu(II), Zn(II) and other metal cation surface complexes in each other's presence. While increased surface retention in each other's presence has been well established, recently published data on zinc and arsenate co-sorption kinetics by our group have shown that As(V) sorbed on goethite in the presence of Zn(II) was less stable and prone to H^+ promoted dissolution at pH 4 and 5.5. Such behavior contradicts the known pH dependence of As(V) adsorption on variably charged surfaces and requires further attention.

Acknowledgments

The authors are grateful for the assistance received from Dr. Pandya (beamline X11a, NSLS) for the collection of EXAFS data. Markus Gräfe appreciates the support of a University of Delaware competitive graduate fellowship for this work.

References

[1] R.S. Oremland, J.F. Stolz, Science 300 (2003) 939–944.
[2] E. Smith, R. Naidu, A.M. Alston, Adv. Agr. 64 (1998) 149–195.
[3] S. Tamaki, W.T. Frankenberger Jr., Rev. Environ. Contam. Toxicol. (Springer-Verlag, New York) 124 (1992) 79–110.
[4] P. O'Day, Elements 2 (2) (2006) 77–83.
[5] S. Fendorf, M.J. Eick, P. Grossl, et al., Environ. Sci. Technol. 31 (2) (1997) 315–320.
[6] Y. Arai, E.J. Elzinga, D.L. Sparks, J. Colloid Interface Sci. 235 (1) (2001) 80–88.
[7] Y. Arai, D.L. Sparks, Soil Sci. 167 (5) (2002) 303–314.
[8] S.R. Randall, D.M. Sherman, K.V. Ragnarsdottir, Geochim. Cosmochim. Acta 65 (7) (2001) 1015–1023.
[9] S.E. O'Reilly, D.G. Strawn, D.L. Sparks, Soil Sci. Soc. Am. J. 65 (1) (2001) 67–77.
[10] G.A. Waychunas, B.A. Rea, C.C. Fuller, et al., Geochim. Cosmochim. Acta 57 (1993) 2251–2269.
[11] P.R. Grossl, M. Eick, D.L. Sparks, et al., Environ. Sci. Technol. 31 (2) (1997) 321–326.
[12] A.C.Q. Ladeira, V.S.T. Ciminelli, H.A. Duarte, et al., Geochim. Cosmochim. Acta 65 (8) (2001) 1211–1217.
[13] S. Goldberg, C.T. Johnston, J. Colloid Interface Sci. 234 (1) (2001) 204–216.
[14] Y. Arai, D.L. Sparks, J. Colloid Interface Sci. 241 (2) (2001) 317–326.
[15] A. Manceau, L. Charlet, J. Colloid Interface Sci. 164 (1994) 87–93.
[16] A. Manceau, Geochim. Cosmochim. Acta 59 (1995) 3647–3653.
[17] D.M. Sherman, S.R. Randall, Geochim. Cosmochim. Acta 67 (22) (2003) 4223–4230.
[18] K.I. Pandya, Phys. Rev. B 50 (21) (1994) 15509–15515.
[19] A.L. Foster, G.E. Brown Jr., T.N. Tingle, et al., Am. Mineral. 83 (1998) 553–568.

[20] M. Gräfe, D.L. Sparks, Geochim. Cosmochim. Acta 69 (19) (2005) 4573–4595.
[21] A.L. Foster, G.E. Brown Jr., G.A. Parks, Geochim. Cosmochim. Acta 67 (11) (2003) 1937–1953.
[22] G.A. Waychunas, C.C. Fuller, J.A. Davis, Geochim. Cosmochim. Acta 66 (7) (2002) 1119–1137.
[23] T.P. Trainor, J.P. Fitts, A.S. Templeton, et al., J. Colloid Interface Sci. 244 (2001) 239–244.
[24] T.P. Trainor, G.E. Brown Jr., G.A. Parks, J. Colloid Interface Sci. 231 (2000) 359–372.
[25] P. Trivedi, L. Axe, T.A. Tyson, J. Colloid Interface Sci. 244 (2) (2001) 230–238.
[26] M. Gräfe, M. Nachtegaal, D.L. Sparks, Environ. Sci. Technol. 38 (24) (2004) 6561–6570.
[27] G.A. Waychunas, B.A. Rea, J.A. Davis, et al., Geochim. Cosmochim. Acta 59 (1995) 3655–3661.
[28] A. Manceau, M.A. Marcus, N. Tamura, in: P. Fenter, N.C. Sturchio (Eds.), Applications of Synchrotron Radiation in Low-Temperature Geochemistry and Environmental Science, in: Rev. Miner. Geochem., vol. 49, Mineral. Soc. Am., Washington, DC, 2002, pp. 341–428.
[29] T. Ressler, J. Synch. Rad. 5 (1998) 118–122.
[30] G. Bunker, Overview of the standard XAFS data analysis procedure, http://gbxafs.iit.edu/training/tutorials.html, 2003, 04/2004.
[31] F. Zabinsky, J.J. Rehr, A. Ankudinov, et al., Phys. Rev. B Condens. Mater. 52 (1995) 2995–3009.
[32] D. Ginderow, F. Cesborn, Acta Crystallogr. B 37 (5) (1981) 1040–1043.
[33] R.J. Hill, Am. Mineral. 61 (9/10) (1976) 979–986.
[34] P. Keller, H. Hess, H. Riffel, Neues Jahrb. Mineral. Abh. 138 (3) (1980) 316–332.
[35] R.L. Frost, L. Duong, W. Martens, Neues Jahrb. Mineral. Monatsh. (5) (2003) 223–240.
[36] P.C. Burns, F.C. Hawthorne, Can. Mineral. 33 (1995) 885–888.
[37] K. Toman, Acta Crystallogr. B 33 (8) (1977) 2628–2631.
[38] P. Keller, H. Hess, Neues Jahrb. Mineral. Abh. 133 (1978) 291–302.
[39] R.K. Eby, F.C. Hawthorne, Acta Crystallogr. C 46 (1990) 2291–2294.
[40] P.C. Burns, R.K. Eby, F.C. Hawthorne, Acta Crystallogr. C 47 (1991) 916–919.
[41] K. Kitahama, R. Kiriyama, B. Yoshihisa, Acta Crystallogr. B 31 (1975) 322–324.
[42] E.A. Stern, Phys. Rev. B 48 (1993) 9825–9827.
[43] D.C. Bull, P.W. Harland, C. Vallance, et al., J. Wood Sci. 46 (3) (2000) 248–252.
[44] B.K. Teo, EXAFS: Basic Principles and Data Analysis, Springer-Verlag, Berlin, 1986.
[45] R.M. Cornell, U. Schwertmann, The Iron Oxides, VCH Verlagsgesellschaft mbH, Weinheim, 1996.
[46] M.B. McBride, Environmental Chemistry of Soils, Oxford Univ. Press, New York, 1994.
[47] X.H. Sun, H.E. Doner, Soil Sci. 161 (12) (1996) 865–872.
[48] M.L. Schlegel, A. Manceau, L. Charlet, J. Phys. IV 7 (C2) (1997) 823–824.
[49] R.H. Parkman, J.M. Charnock, N.D. Bryan, et al., Am. Mineral. 84 (3) (1999) 407–419.
[50] L. Bochatay, P. Persson, L. Lovgren, et al., J. Phys. IV 7 (C2) (1997) 819–820.
[51] C.L. Peacock, D.M. Sherman, Geochim. Cosmochim. Acta 68 (12) (2004) 2623–2637.
[52] R.D. Shannon, Acta Crystallogr. A 32 (Sep1) (1976) 751–767.